Identification of nonclassical light with multiplexing layouts and arbitrary detectors

J. Sperling,[1,*] A. Eckstein,[1] W. R. Clements,[1] M. Moore,[1] J. J. Renema,[1] W. S. Kolthammer,[1] S. W. Nam,[2] A. Lita,[2] T. Gerrits,[2] I. A. Walmsley,[1] G. S. Agarwal,[3] and W. Vogel[4]

[1] *Clarendon Laboratory, University of Oxford, Parks Road, Oxford OX1 3PU, United Kingdom*
[2] *National Institute of Standards and Technology, 325 Broadway, Boulder, CO 80305, USA*
[3] *Texas A&M University, College Station, Texas 77845, USA*
[4] *Institut für Physik, Universität Rostock, Albert-Einstein-Straße 23, D-18059 Rostock, Germany*

(Dated: December 21, 2016)

In our work [1], we introduce and apply a detector-independent method to uncover nonclassicality. In this contribution, we extend those techniques and give more details on the performed analysis. We derive the general structure of the positive-operator-valued measurement operators that describe multiplexing layouts with arbitrary detectors. From the resulting quantum version of multinomial statistics, we infer nonclassicality probes based on a matrix of normally ordered moments. We discuss these criteria and apply them to our data which are measured with superconducting transition-edge sensors. Our experiment produces heralded multi-photon states from a parametric down-conversion light source. We show that the notions of sub-Poisson and sub-binomial light can be deduced from our general approach and we establish the concept of sub-multinomial light, which is shown to outperform the former two concepts of nonclassicality for our data.

I. INTRODUCTION

The bare existence of photons highlights the particle nature of electromagnetic waves in quantum optics [2]. Therefore, the generation and detection of photon states are crucial for a comprehensive understanding of fundamental concepts in quantum physics; see Refs. [3, 4] for recent reviews on single photons. Beyond this scientific motivation, the study of nonclassical radiation fields is also of practical importance. For instance, quantum communication protocols rely on the generation and detection of photons [5, 6]. Yet, unwanted attenuation effects—which are always present in realistic scenarios—results in a decrease of the nonclassicality of a produced light field. Conversely, an inappropriate detector model can introduce fake-nonclassicality even to a classical radiation field [7–9]. For this reason, we seek for robust and detector-independent certifiers of nonclassicality.

The basic definition of nonclassicality is that a quantum state of light cannot be described in terms of classical statistical optics. A convenient way to represent general states is given in terms of the Glauber-Sudarshan P function [10, 11]. Whenever this distribution cannot be interpreted in terms of classical probability theory, the thereby represented state is a nonclassical one [12, 13]. A number of nonclassicality tests have been proposed; see Ref. [14] for an overview. Most of them are formulated in terms of matrices of normally ordered moments of physical observables; cf., e.g., [15]. For instance, the concept of nonclassical sub-Poisson light [16] can be written and even generalized in terms of matrices of higher-order photon-number correlations [17]. Other matrix-based nonclassicality tests employ the Fourier or Laplace transform of the Glauber-Sudarshan P function [18, 19].

In order to apply such nonclassicality probes, one has to measure the light field under study with a photodetector [20, 21]. The photon statistics of the measured state can be inferred if the used detector has been properly characterized. This can be done by a detector tomography [22–26]—i.e., measuring a comparably large number of well-defined probe states to construct a detection model. Alternatively, one can perform a detector calibration [27–29]—i.e., the estimation of parameters of an existing detection model with some reference measurements. Of particular interest are photon-number-resolving detectors of which superconducting transition-edge sensors (TESs) are a successful example [30–34]. Independent of the particular realization, photon-number-resolving devices allow for the implementation of quantum tasks, such as state reconstruction [35, 36], imaging [37, 38], random number generation [39], and the characterization of sources of nonclassical light [40–43]—even in the presence of strong imperfections [44]. Moreover, higher-order [45–47], spatial [48, 49], and conditional [50] quantum correlations have been studied.

So far, we did not distinguish between the detection scheme and the actual detectors. That is, one has to discern the optical manipulation of a signal field and its interaction with a sensor which yields a measurement outcome. Properly designed detection layouts of such a kind render it possible to infer or use properties of quantum light without having a photon-number-resolution capability [51–53] or they do not require a particular detector model [54, 55]. For instance, multiplexing layouts with a number of detectors that can only discern between the presence ("on") or absence ("off") of absorbed photons can be combined into a photon-number-resolving detection device [56–60]. Such types of schemes use an optical network to split an incident light field into a number of spatial or temporal modes which are subsequently measured with on/off detectors. The measured statistics is shown to resemble a binomial distribution [9] rather than

* jan.sperling@physics.ox.ac.uk

a Poisson statistics, which is obtained for photoelectric detection models [61]; see also [62, 63] in this context. For such detectors, the positive operator-valued measure (POVM), which fully describes the detection layout, has been formulated [9, 64]. Recently, the combination of a multiplexing scheme with multiple TESs has been used to significantly increase the photon-number resolution [65].

Based on the binomial character of the statistics of multiplexing layouts with on/off detectors, the notion of sub-binomial light has been introduced [66] and experimentally demonstrated [67]. It replaces the earlier mentioned concept of sub-Poisson light [16] that applies to photoelectric counting models [61]. Note that nonclassical light can be similarly inferred from devices based on unbalanced multiplexing (i.e., non-identical splitting ratios) [68]. In addition, the on-chip realization of optical networks [69] can be used to produce integrated detection schemes to verify sub-binomial light [70].

In this work, we derive the quantum-optical click-counting statistics for multiplexing layouts which employ arbitrary detectors. Consequently, we formulate detector-independent nonclassicality tests in terms of normally-ordered moments. This method is applied to our experiment which produces heralded multi-photon states. Our results are discussed in relation with other notions of nonclassical photon correlations.

In our Letter [1], we study the same topic as we do in this work from a classical perspective. There, the treatment of the detector-independent verification of quantum light is performed solely in terms of classical statistical optics. Here, however, we use a complementary quantum-optical perspective on this topic. Beyond that, we also consider additional features of our measurements, give details on the statistical analysis (fully presented in Appendix A) and compare our results with simple theoretical models (given in Appendix B).

This work is organized as follows. In Sec. II, the detector-independent model for our detection layout is elaborated. Section III includes the derivation and the discussion of the nonclassicality conditions. We give a brief overview of the performed experiment in Sec. IV with special emphasis on the used TESs. An extended analysis of our data, presented in Sec. V, includes the comparison of different forms of nonclassicality. We summarize and conclude in Sec. VI.

II. DETECTION MODEL

We begin with the derivation of the detector-independent formulation of a theoretical model for the measurement layout under study (Fig. 1). This optical detection scheme consists of a multiplexing network which splits a signal into N modes. Those outputs are measured with N identical detectors which can produce $K+1$ outcomes labeled as 0, ..., K. Let us stress that we make a clear distinction between the well-characterized optical multiplexing, the individual and unspecified detectors, and the resulting full detection scheme. We will use the standard calculus in quantum optics which is based on bosonic operator ordering; see [71] for an detailed introduction.

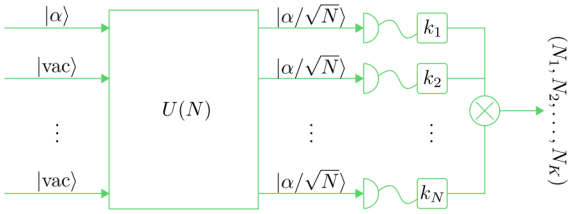

FIG. 1. (Color online) Outline of the multiplexing scheme for a coherent state $|\alpha\rangle$. A balanced optical network—represented by the unitary $U(N)$—splits the incident coherent state $|\alpha\rangle$ into $|\alpha/\sqrt{N}\rangle^{\otimes N}$. The individual detectors give an outcome $k_n \in \{0, \ldots, K\}$. The number of detectors which deliver the same outcome k defines N_k.

In the multiplexing scheme, an input coherent state $|\alpha\rangle$ is distributed over N output modes. Further on, we have vacuum $|\mathrm{vac}\rangle = |0\rangle$ at all other $N-1$ input ports. In general, the N input modes—defined by the bosonic annihilation operators $\hat{a}_n$—are transformed via the unitary $U(N) = (U_{m,n})_{m,n=1}^{N}$ into the output modes

$$\hat{b}_m = U_{m,1}\hat{a}_1 + \cdots + U_{m,N}\hat{a}_N. \tag{1}$$

The optical network does a balanced splitting, $|U_{n,m}|^2 = 1/N$. We can also employ local phase rotations $e^{i\varphi_m}\hat{b}_m$ to get, without a loss of generality, $U_{m,1} = |U_{m,1}| = 1/\sqrt{N}$ for $1 \leq m \leq N$. Hence, we have the following input-output relation

$$|\alpha\rangle \otimes |0\rangle^{\otimes(N-1)} \overset{U(N)}{\longmapsto} |\alpha/\sqrt{N}\rangle \otimes \cdots \otimes |\alpha/\sqrt{N}\rangle. \tag{2}$$

Note that a balanced, but lossy network similarly yields $|\tau\alpha\rangle \otimes \cdots \otimes |\tau\alpha\rangle$ for $\tau \leq 1/\sqrt{N}$.

For describing the detector, we cannot make any specifications as we did for the optical multiplexing. The probability p_k for the kth measurement outcome ($0 \leq k \leq K$) for any type of detector can be written in terms of the expectation value of the POVM operators $:\hat{\pi}_k':$. That is $p_k = \langle :\hat{\pi}_k': \rangle$, where $:\cdots:$ denotes the normal-ordering prescription. Note that any operator can be written in such a form. In addition, we may recall that expectation values of normally-ordered operators and coherent states can be simply computed by replacing the bosonic annihilation and creation operator with the coherent amplitude and their complex conjugate, respectively. For the coherent states $|\alpha/\sqrt{N}\rangle$, we have

$$p_k(\alpha) = \langle \alpha/\sqrt{N}|:\hat{\pi}_k':|\alpha/\sqrt{N}\rangle = \langle \alpha|:\hat{\pi}_k:|\alpha\rangle, \tag{3}$$

whereby we also define $:\hat{\pi}_k:$ in terms of $:\hat{\pi}_k':$ through the mapping $\hat{a} \mapsto \hat{a}/\sqrt{N}$.

We find for a measurement with our N detectors and our coherent output state (2) that the probability to measure the outcome k_n with the nth detector—more rigorously a coincidence $(k_1,\ldots,k_N)$—is given by

$$p_{k_1}(\alpha)\cdots p_{k_N}(\alpha)=\langle\alpha|{:}\hat{\pi}_{k_1}\cdots\hat{\pi}_{k_N}{:}|\alpha\rangle, \tag{4}$$

where we used Eq. (3) and the following relation for normal ordering: $\langle\alpha|{:}\hat{A}{:}|\alpha\rangle\langle\alpha|{:}\hat{B}{:}|\alpha\rangle=\langle\alpha|{:}\hat{A}\hat{B}{:}|\alpha\rangle$ for any two (or more) operators $\hat{A}$ and $\hat{B}$. The Glauber-Sudarshan representation [10, 11] allows one to expand any quantum state as a quasi-mixture of coherent states, $\hat{\rho}=\int d^2\alpha\,P(\alpha)|\alpha\rangle\langle\alpha|$. Thus, we can write for any $\hat{\rho}$

$$\begin{aligned}p_{(k_1,\ldots,k_N)}&=\int d^2\alpha\,P(\alpha)p_{k_1}(\alpha)\cdots p_{k_N}(\alpha)\\&=\langle{:}\hat{\pi}_{k_1}\cdots\hat{\pi}_{k_N}{:}\rangle.\end{aligned} \tag{5}$$

So far we studied the individual parts, i.e., the optical multiplexing and the N individual detectors. For the combination of both to describe the setup in Fig. 1, we need some combinatorics. Suppose N_k is the number of elements of $(k_1,\ldots,k_N)$ which take the value k. Then, $(N_0,\ldots,N_K)$ describes the coincidence that N_0 detectors yield the outcome 0, N_1 detectors yield the outcome 1, etc. One specific measurement outcome is defined by $(k_{0,1},\ldots,k_{0,N})$,

$$k_{0,n}=\begin{cases}0 & \text{for} \quad 1\leq n\leq N_0,\\ 1 & \text{for} \quad N_0+1\leq n\leq N_0+N_1,\\ \vdots & \\ K & \text{for} \quad N_0+\cdots+N_{K-1}+1\leq n\leq N,\end{cases} \tag{6}$$

which results in $(N_0,\ldots,N_K)$, where the total number of detectors is $N=N_0+\cdots+N_K$. This specific example can be used to represent all similar outcomes as we will show now. The $(k_1,\ldots,k_N)$ for the same combination $(N_0,\ldots,N_K)$ can be obtained from $(k_{0,\sigma(1)},\ldots,k_{0,\sigma(N)})$ via a permutation $\sigma\in\mathcal{S}_N$ of the elements. Here $\mathcal{S}_N$ denotes the permutation group of N elements which has a cardinality of $N!$. Note that all permutations σ which exchange identical outcomes result in the same tuple. This means for the outcome defined in Eq. (6) that $(k_{0,\sigma(1)},\ldots,k_{0,\sigma(N)})=(k_{0,1},\ldots,k_{0,N})$ for any permutation of the form $\sigma\in\mathcal{S}_{N_0}\times\cdots\times\mathcal{S}_{N_K}$. Therefore, the POVM element for a given $(N_0,\ldots,N_K)$ can be obtained by summing over all permutations $\sigma\in\mathcal{S}_N$ of the POVMs of individual outcomes ${:}\hat{\pi}_{k_{0,1}}\cdots\hat{\pi}_{k_{0,N}}{:}$ [Eq. (5)] while correcting for the $N_0!\cdots N_K!$ multi-counts. More rigorously, we can write

$$\begin{aligned}\hat{\Pi}_{(N_0,\ldots,N_K)}&=\frac{1}{N_0!\cdots N_K!}\sum_{\sigma\in\mathcal{S}_N}{:}\hat{\pi}_{k_{0,\sigma(1)}}\cdots\hat{\pi}_{k_{0,\sigma(N)}}{:}\\&=\frac{N!}{N_0!\cdots N_K!}{:}\hat{\pi}_0^{N_0}\cdots\hat{\pi}_K^{N_K}{:},\end{aligned} \tag{7}$$

where relations of the form ${:}\hat{A}\hat{B}\hat{A}{:}={:}\hat{A}^2\hat{B}{:}$ have been used.

In conclusion, we get for the detection layout in Fig. 1 the click counting statistics of a state $\hat{\rho}$ as

$$\begin{aligned}c_{(N_0,\ldots,N_K)}&=\mathrm{tr}[\hat{\rho}\hat{\Pi}_{(N_0,\ldots,N_K)}]\\&=\left\langle{:}\frac{N!}{N_0!\cdots N_K!}\hat{\pi}_0^{N_0}\cdots\hat{\pi}_K^{N_K}{:}\right\rangle,\end{aligned} \tag{8}$$

which is a normally-ordered version of a multinomial statistics. Using the Glauber-Sudarshan representation, we can also write

$$\begin{aligned}c_{(N_0,\ldots,N_K)}=\int d^2\alpha\,P(\alpha)&\frac{N!}{N_0!\cdots N_K!}\\&\times p_0(\alpha)^{N_0}\cdots p_K(\alpha)^{N_K}.\end{aligned} \tag{9}$$

In this form, we can directly observe that any classical statistics, $P(\alpha)\geq 0$, is a classical average over multinomial probability distributions; see also [1].

In this section, we derived the click-counting statistics (8) for unspecified POVMs of the individual detectors. This was achieved by using the properties of a well-defined optical multiplexing scheme. We solely assumed that the N detectors are described by the same $K+1$ POVMs. Hence, the resulting full detection scheme was shown to result always in a quantum version of multinomial statistics. This also holds for an infinite, countable $(K=|\mathbb{N}|)$ or even uncountable $(K=|\mathbb{R}|)$ set of outcomes, for which any measurement run can only deliver a finite sub-sample. For coherent light $|\alpha_0\rangle$, the statistics actually becomes a true multinomial probability distribution; see Eq. (9) for $P(\alpha)=\delta(\alpha-\alpha_0)$. In the case of a binary outcome, $K+1=2$, we get the binomial distribution which has been derived and generalized in Refs. [9, 72] and applies, for example, to avalanche photodiodes in the Geiger mode. In contrast to our work [1], we used here a full quantum-optical approach to derive the general form of the click statistics.

III. NONCLASSICALITY CRITERIA

Our click-counting model (8) describes a multiplexing scheme and employs arbitrary detectors. It is based on normally ordered expectation values of the form $\langle{:}\hat{\pi}_0^{m_0}\cdots\hat{\pi}_K^{m_K}{:}\rangle$. Hence, we can formulate nonclassicality criteria in terms of such moments. For this reason, let us recall that any classical state obeys [73]

$$0\overset{\text{cl.}}{\leq}\langle{:}\hat{f}^\dagger\hat{f}{:}\rangle. \tag{10}$$

We expand $\hat{f}=\sum_{m_0+\cdots+m_K\leq N/2}f_{m_0,\ldots,m_K}\hat{\pi}_0^{m_0}\cdots\hat{\pi}_K^{m_K}$, which is chosen such that it solely includes the operators that are actually measured. Therefrom, we get

$$\begin{aligned}\langle{:}\hat{f}^\dagger\hat{f}{:}\rangle=&\sum_{\substack{m_0+\cdots+m_K\leq N/2\\ m_0'+\cdots+m_K'\leq N/2}}f^*_{m_0,\ldots,m_K}\\&\times\left\langle{:}\hat{\pi}_0^{m_0+m_0'}\cdots\hat{\pi}_K^{m_K+m_K'}{:}\right\rangle f_{m_0',\ldots,m_K'}\\=&\vec{f}^\dagger M\vec{f},\end{aligned} \tag{11}$$

with a vector $\vec{f} = (f_{m_0,\ldots,m_K})_{(m_0,\ldots,m_K)}$, using a multi-index notation, and the matrix of normally ordered moments M, which is defined in terms of the elements $\langle{:}\hat{\pi}_0^{m_0+m_0'}\cdots\hat{\pi}_K^{m_K+m_K'}{:}\rangle$. As the non-negativity of the above expression holds for classical states and for all coefficients $\vec{f}$, we can equivalently write: A state is nonclassical if

$$0 \not\leq M. \tag{12}$$

Also note that the total power of $\langle{:}\hat{\pi}_0^{m_0+m_0'}\cdots\hat{\pi}_K^{m_K+m_K'}{:}\rangle$ is bounded by the number of individual detectors, $N \geq m_0+\cdots+m_K+m_0'+\cdots+m_K'$ as the measured statistics (8) only allows for retrieving such powers.

It can be also shown (Appendix A in Ref. [74]) that the matrix of normally ordered moments can be equivalently expressed in a form that is based on central moments, $\langle{:}(\Delta\hat{\pi}_0)^{m_0+m_0'}\cdots(\Delta\hat{\pi}_K)^{m_K+m_K'}{:}\rangle$. For instance and while restricting to the second-order submatrix, we get nonclassicality conditions in terms of normally-ordered covariances,

$$\begin{aligned} 0 \not\leq M^{(2)} &= \left(\langle{:}\Delta\hat{\pi}_k\Delta\hat{\pi}_{k'}{:}\rangle\right)_{k,k'=0,\ldots,K} \\ &= \begin{pmatrix} \langle{:}(\Delta\hat{\pi}_0)^2{:}\rangle & \cdots & \langle{:}(\Delta\hat{\pi}_0)(\Delta\hat{\pi}_K){:}\rangle \\ \vdots & \ddots & \vdots \\ \langle{:}(\Delta\hat{\pi}_0)(\Delta\hat{\pi}_K){:}\rangle & \cdots & \langle{:}(\Delta\hat{\pi}_K)^2{:}\rangle \end{pmatrix}. \end{aligned} \tag{13}$$

Additionally, the relation $\langle{:}\hat{\pi}_K{:}\rangle = 1 - [\langle{:}\hat{\pi}_0{:}\rangle + \cdots + \langle{:}\hat{\pi}_{K-1}{:}\rangle]$ implies that the last row of $M^{(2)}$ is linearly dependent on the other ones. This further implies that 0 is an eigenvalue of $M^{(2)}$. Hence, we get for any classical state that the minimal eigenvalue of this covariance matrix is necessarily zero.

In order to relate the considered nonclassicality criteria to the measurement of the click-counting statistics (8), let us consider the generating function which is given by

$$\begin{aligned} g(z_0,\ldots,z_N) &= \overline{z_0^{N_0}\cdots z_K^{N_K}} \\ &= \sum_{N_0+\cdots+N_K=N} c_{(N_0,\ldots,N_K)} z_0^{N_0}\cdots z_K^{N_K} \\ &= \left\langle {:}\left(z_0\hat{\pi}_0+\cdots+z_K\hat{\pi}_K\right)^N{:} \right\rangle. \end{aligned} \tag{14}$$

The derivatives of the generating function relate the measured moments with the normally-ordered ones,

$$\begin{aligned} &\partial_{z_0}^{m_0}\cdots\partial_{z_K}^{m_K} g(z_0,\ldots,z_K)\big|_{z_0=\cdots=z_K=1} \\ &= \sum_{N_0+\cdots+N_K=N} c_{(N_0,\ldots,N_K)} \frac{N_0!}{(N_0-m_0)!}\cdots\frac{N_K!}{(N_K-m_K)!} \\ &= \overline{(N_0)_{m_0}\cdots(N_K)_{m_K}} \\ &= (N)_{m_0+\cdots+m_K}\,\langle{:}\hat{\pi}_0^{m_0}\cdots\hat{\pi}_K^{m_K}{:}\rangle \end{aligned} \tag{15}$$

for $m_0+\cdots+m_K \leq N$ and $(x)_m = x(x-1)\cdots(x-m+1) = x!/(x-m)!$ being the falling factorial. The factorial moments $\overline{(N_0)_{m_0}\cdots(N_K)_{m_K}}$ can be directly sampled from the measured $c_{(N_0,\ldots,N_K)}$. With the above relation (15), they can be also connected to normally-ordered moments which are needed for our nonclassicality tests.

As an example and due to its importance, let us focus on the first and second order moments in detail. We obtain

$$\langle{:}\hat{\pi}_k{:}\rangle = \frac{\overline{N_k}}{N} \text{ and } \langle{:}\hat{\pi}_k\hat{\pi}_{k'}{:}\rangle = \frac{\overline{N_kN_{k'}} - \delta_{k,k'}\overline{N_k}}{N(N-1)} \tag{16}$$

for $k,k' \in \{0,\ldots,K\}$. Hence, our covariances are alternatively represented by

$$\langle{:}\Delta\hat{\pi}_k\Delta\hat{\pi}_{k'}{:}\rangle = \frac{N\overline{\Delta N_k\Delta N_{k'}} - \overline{N_k}\left(N\delta_{k,k'} - \overline{N_{k'}}\right)}{N^2(N-1)}. \tag{17}$$

As the corresponding matrix (13) of normally ordered moments is non-negative for classical states, we get

$$\begin{aligned} 0 \overset{\text{cl.}}{\leq} & N^2(N-1)M^{(2)} \\ &= \left(N\overline{\Delta N_k\Delta N_{k'}} - \overline{N_k}\left[N\delta_{k,k'} - \overline{N_{k'}}\right]\right)_{k,k'=0,\ldots,K}. \end{aligned} \tag{18}$$

The violation of this very constraint for classical states has been experimentally demonstrated for the generated quantum light [1].

Let us consider some special cases of the above criterion. In particular, let us study the projections that result in a nonclassicality condition

$$\vec{f}^{\,\mathrm{T}} M^{(2)} \vec{f} < 0 \tag{19}$$

[cf. also Eqs. (10) and (11)]. Note that $M^{(2)}$ is a real-valued and symmetric $(K+1)\times(K+1)$ matrix. Thus, it is sufficient to consider real-valued vectors $\vec{f} = (f_0,\ldots,f_K)^{\mathrm{T}}$. Further on, let us define the operator $:\hat{\mu}: = f_0{:}\hat{\pi}_0{:} + \cdots + f_K{:}\hat{\pi}_K{:}$. Then, we can also read condition (19) as

$$\langle{:}(\Delta\hat{\mu})^2{:}\rangle < 0. \tag{20}$$

This means that the fluctuations of the observable $:\hat{\mu}:$ are below those of any classical light field. In the following, we consider specific choices for $\vec{f}$ to retrieve different nonclassicality criteria.

a. Sub-multinomial light. The minimization of (19) over all normalized vectors yields the minimal eigenvalue Q_{multi} of $M^{(2)}$. That is

$$Q_{\text{multi}} = \min_{\vec{f}:\vec{f}^{\,\mathrm{T}}\vec{f}=1} \vec{f}^{\,\mathrm{T}} M^{(2)} \vec{f} = \vec{f}_0^{\,\mathrm{T}} M^{(2)} \vec{f}_0, \tag{21}$$

where $\vec{f}_0$ is a normalized eigenvector to the minimal eigenvalue. If we have $M^{(2)} \not\geq 0$, then we necessarily get $Q_{\text{multi}} < 0$. For classical states, we get $Q_{\text{multi}} = 0$; see the discussion below Eq. (13). As this criterion exploits the maximal negativity from covariances of the multinomial statistics, we refer to a radiation field with $Q_{\text{multi}} < 0$ as sub-multinomial light. This method has been applied in Ref. [1] (see also Appendix A for the error estimation).

b. Sub-binomial light. We can also consider the vector $\vec{f}=(0,1,\ldots,1)^{\mathrm{T}}$. This yields $:\hat{\mu}:=\hat{1}-:\hat{\pi}_0:$. Hence, we effectively reduce our system to a detection with a binary outcome. Using a proper scaling, we get

$$\begin{aligned}\frac{(N-1)\vec{f}^{\mathrm{T}}M^{(2)}\vec{f}}{\langle:\hat{\pi}_0:\rangle(1-\langle:\hat{\pi}_0:\rangle)}&=\frac{N\overline{(\Delta B)^2}-N\overline{B}+\overline{B}^2}{(N-\overline{B})\overline{B}}\\ =N\frac{\overline{(\Delta B)^2}}{\overline{B}(N-\overline{B})}-1&=Q_{\mathrm{bin}},\end{aligned}\tag{22}$$

with $B=N_1+\cdots+N_K=N-N_0$ and using Eq. (17). The condition $Q_{\mathrm{bin}}<0$ defines the notion of sub-binomial light [66] and is found to be a special case of our general relation.

c. Sub-Poisson light. Finally, we study the criterion (19) for a vector $\vec{f}=(0,1,\ldots,K)^{\mathrm{T}}$. We have $:\hat{\mu}:=\sum_{k=0}^{K}k:\hat{\pi}_k:$ and we also define

$$A=\sum_{k=0}^{K}kN_k.\tag{23}$$

Their mean values are related to each other,

$$\langle:\hat{\mu}:\rangle=\sum_{k=0}^{K}k\frac{\overline{N_k}}{N}=\frac{\overline{A}}{N}.\tag{24}$$

We point out that $\overline{N_k}/N$ can be also interpreted as probabilities, with $N=N_0+\cdots+N_K=\overline{N_0}+\cdots+\overline{N_K}$. Further, we can write the normally-ordered variance in the form

$$\begin{aligned}&\vec{f}^{\mathrm{T}}M^{(2)}\vec{f}=\langle:(\Delta\mu)^2:\rangle\\ =&\frac{\overline{(\Delta A)^2}-\overline{A}}{N(N-1)}\\ &-\frac{\left(\sum_{k=0}^{K}k^2\frac{\overline{N_k}}{N}\right)-\left(\sum_{k=0}^{K}k\frac{\overline{N_k}}{N}\right)^2-\left(\sum_{k=0}^{K}k\frac{\overline{N_k}}{N}\right)}{N-1}.\end{aligned}\tag{25}$$

We can now conclude that

$$\begin{aligned}\frac{\langle:(\Delta\mu)^2:\rangle}{\langle:\mu:\rangle}&=\frac{Q_{\mathrm{Pois}}-Q'_{\mathrm{Pois}}}{N-1},\ \text{with}\ Q_{\mathrm{Pois}}=\frac{\overline{(\Delta A)^2}}{\overline{A}}-1\\ \text{and}\ Q'_{\mathrm{Pois}}&=\frac{\left(\sum_{k=0}^{K}k^2\frac{\overline{N_k}}{N}\right)-\left(\sum_{k=0}^{K}k\frac{\overline{N_k}}{N}\right)^2}{\left(\sum_{k=0}^{K}k\frac{\overline{N_k}}{N}\right)}-1.\end{aligned}\tag{26}$$

The parameters $Q^{(\prime)}_{\mathrm{Pois}}$ relate to the notion of sub-Poisson light [16]. However, we have a difference of two such Mandel parameters in Eq. (26). The second parameter Q'_{Pois} can be considered as a correction, because the statistics of A is only in a rough approximation a Poisson distribution. Let us clarify this.

Let us assume a detector that allows for the resolution of $K=\infty$ measurement outcomes, which are related to measurement operators of a Poisson form, $:\hat{\pi}'_k:=:\hat{\Gamma}^k e^{-\hat{\Gamma}}:/k!$ [61], where $\hat{\Gamma}=\eta\hat{n}$ is an example of a linear detector response function (η quantum efficiency). Using the definition (3), we get $:\hat{\pi}_k:=:(\hat{\Gamma}/N)^k e^{-\hat{\Gamma}/N}:/k!$, where the denominator N accounts for the splitting into N modes [72]. This idealized model yields $\langle:\hat{\mu}:\rangle=\langle:(\hat{\Gamma}/N):\rangle$ and

$$\sum_{k=0}^{\infty}k^2\frac{\overline{N_k}}{N}=\frac{\langle:\hat{\Gamma}^2:\rangle}{N^2}+\frac{\langle:\hat{\Gamma}:\rangle}{N}\ \text{and}\ \overline{A^2}=\langle:\hat{\Gamma}^2:\rangle+\langle:\hat{\Gamma}:\rangle.\tag{27}$$

Hence, we have $Q_{\mathrm{Pois}}=\langle:(\Delta\hat{\Gamma})^2:\rangle/\langle:\hat{\Gamma}:\rangle=NQ'_{\mathrm{Pois}}$ and

$$\frac{\langle:(\Delta\mu)^2:\rangle}{\langle:\mu:\rangle}=\frac{1}{N}Q_{\mathrm{Pois}}.\tag{28}$$

Thus, we have shown that for photoelectric detection models, we retrieve the notation of sub-Poisson light, $Q_{\mathrm{Pois}}<0$, from the general form (26), which includes a correction term.

In this section, we formulated nonclassicality tests which are designed such that they can be directly sampled from the data obtained from the measurement layout in Fig. 1. Especially, we focused on the second-order nonclassicality probes. In the following, we will apply them to our data. We will compare the cases of sub-multinomial [Eq. (21)], sub-binomial [Eq. (22)], and (corrected) sub-Poisson [Eq. (26)] light. Before doing this, we describe the experiment and study some non-trivial features of our individual detectors.

IV. EXPERIMENT

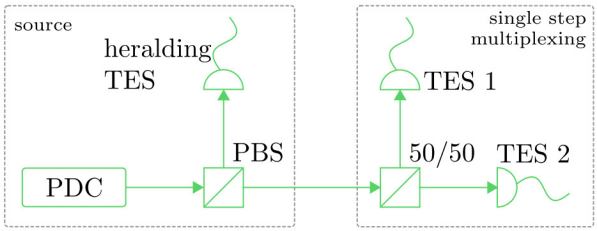

FIG. 2. (Color online) Schematic setup. A parametric down-conversion (PDC) source emits photon pairs which are separated with a polarizing beam splitter (PBS). Conditioned on the measurement outcome of the heralding TES, different photon-number states are produced. A single multiplexing step is realized by splitting the photon states on a balanced 50/50 beam splitter and subsequently we detect them with two TESs.

An outline of our setup is given in Fig. 2. It is divided into a source that produces heralded photon states and a detection stage which represents one multiplexing step. In total, we use three superconducting TESs. For generating correlated photons, we employ a spontaneous parametric down-conversion (PDC) source. In this section, we describe the individual parts in some more detail.

a. The PDC source. Our spontaneous PDC source is a waveguide-written periodically poled potassium titanyl phosphate (PP-KTP) crystal which is 8 mm long. The type-II spontaneous PDC process is pumped with laser pulses at 775 nm and a full width at half maximum (FWHM) of 2 nm at a repetition rate of 75 kHz. The heralding idler mode has a horizontal polarization and it is centered at 1554 nm. The signal mode is vertically polarized and centered at 1546 nm. A PBS spatially separates the output signal and idler pulses. An edge filter discards the pump beam. In addition, the signal and idler are filtered by a 3 nm bandpass filters. This is done in order to filter out the broadband background which is typically generated in dielectric nonlinear waveguides [75]. In general, such PDC sources have been proven to be well-understood and reliable sources of quantum light [76, 77]. Hence, we may focus our attention on the employed detectors.

b. The TES detectors. We use superconducting TESs [30] as our photon detectors. These TESs are micro-calorimeters consisting of $25\,\mu\text{m} \times 25\,\mu\text{m} \times 20\,\text{nm}$ slabs of tungsten located inside an optical cavity with a gold backing mirror designed to maximize absorption at the desired wavelengths. They are secured within a ceramic ferule as part of a self-aligning mounting system, so that the fiber core is well aligned to the center of the detector [78]. The TESs are first cooled below their transition temperature within a dilution refrigerator and then heated back up to their transition temperature by Joule heating caused by a voltage bias, which is self-stabilized via an electro-thermal feedback effect [79]. Within this transition region, the steep resistance curve ensures that the small amount of heat deposited by photon absorption causes a measurable decrease in current flowing through the device. After photon absorption, the heat is then dissipated to the environment via a weak thermal link to the TES substrate.

To read out the signal from this photon absorption process, the current change—produced by photon absorption in the TES—is inductively coupled to a superconducting quantum interference device (SQUID) module where it is amplified, and this signal is subsequently amplified at room temperature. This results in complex time-varying signals of about $5\,\mu\text{s}$ duration. These signals are sent to a digitizer to perform fast analogue-to-digital conversion, where the overlap with a reference signal is computed and then binned. This method allows us to process incoming signals at a speed of up to 100 kHz.

Our TESs are installed in a dilution refrigerator operating at a base temperature of about 70 mK and a cooling power of $400\,\mu\text{W}$ at 100 mK. One of the detectors has a measured detection efficiency of $0.98^{+0.02}_{-0.08}$ [80]. The other two TESs have identical efficiencies within the error of our estimation.

c. Detector response analysis. Even though we will not use specific detector characteristics for our analysis of nonclassicality, it is nevertheless scientifically interesting to study their response. This will also outline the complex behavior of superconducting detectors. For the time being, we ignore the detection events of the TESs 1 and 2 in Fig. 2 and solely focus on the measurement of the heralding TES. In Fig. 3, the measurement outcome of those marginal counts is shown. We can see that we can resolve the bins $k \in \{0, \ldots, 11\}$ (cf. also [1]). The distribution around the peaked structures can be considered as fluctuations of the energy levels (indicated by vertical dark green, solid lines). We observe that the difference between two discrete energies E_n is not constant as one would expect from $E_{n+1} - E_n = \hbar\omega$, which will be treated in the next paragraph. In addition, the marginal photon statistics should be given by a geometric distribution for the two-mode squeezed-vacuum state produced by our PDC source; see Appendix B. In the logarithmic scaling in Fig. 3, this would result in a linear function. However, we observe a deviation from such a model; compare light green, dashed and dot-dashed lines in Fig. 3.

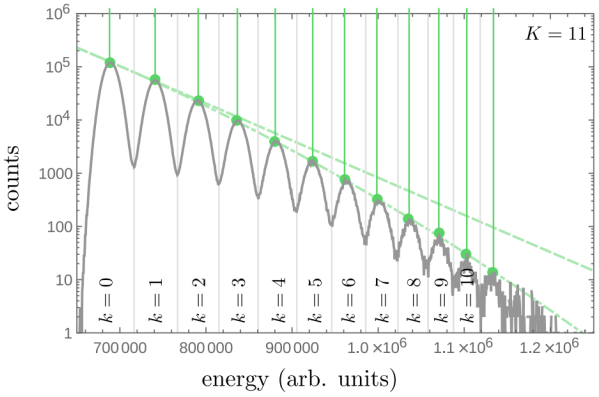

FIG. 3. (Color online) The counts of the heralding TES (solid, gray curve). Maxima for all $K = 11$ bins are shown as bullets. The dark vertical lines give the energy levels of the maxima. A nonlinear regression ($\log_{10} y = ax^2 + bx + c$; dot-dashed line) and its tangent at the first maximum (dashed line) are additionally shown.

This deviation from the expected, linear behavior could have two origins: The source is not producing a two-mode squeezed-vacuum state (affecting the height of the peaks). Or the detector, including the SQUID response, is not operating in a linear detection regime (influence on the horizontal axis). To counter the latter point, the measured energies E and the position of the peaks—considered to be the photon numbers n—have been fitted by a quadratic response function $n = aE^2 + bE + c$; see the inset in Fig. 4. As a result of such a calibration, the peaked structure is well-described by a linear function in n for the heralding TES as shown in Fig. 4 (top), which is now consistent with the theoretical expectation. The same nonlinear transformation also yields a linear n-dependence for the TESs 1 and 2 (cf. Fig. 4, bottom). Note that those two detectors only allow for a resolution of $K + 1 = 8$ bins and that these two detectors have indeed a very similar response—the

depicted linear function is identical for both. In conclusion, it is more likely that the measured nonlinear behavior in Fig. 4 can be assigned to the detectors; and the PDC source is operating according to our expectations.

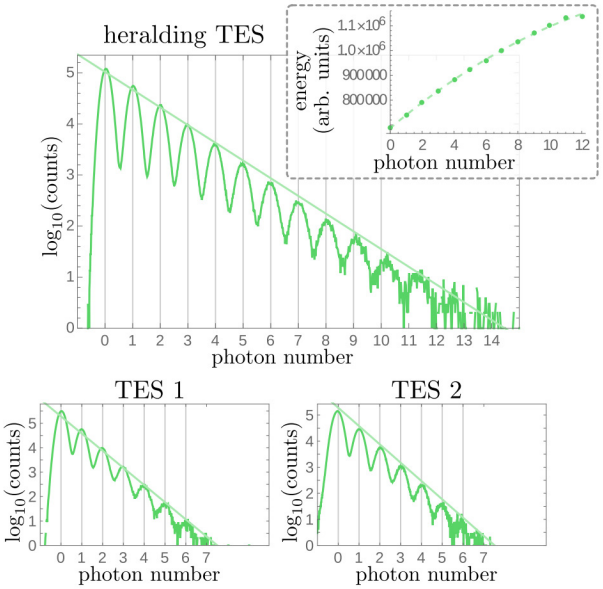

FIG. 4. (Color online) A possible assignment between the measured counts and the photon number estimate is shown for all TESs. As an example, the curve in the dashed box serves as the conversion from the measured energies of the heralding TES (points depict the maxima from Fig. 3). This conversion yields an almost exponential ($\log_{10} y = ax + b$, light green lines) decay of the counts as it is expected for the geometric statistics.

As we discussed initially, we encountered an unexpected, nonlinear behavior of our data. To correct for this, we use the fact that the marginal photon-number distribution of our source is an exponential one to make some predictions about the detector response in a particular interval. However, a lack of such extra knowledge prevents one from characterizing the detector or from eventually concluding nonclassicality. Here, we have formulated detector-independent nonclassicality tests to circumvent this deficiency. They are accessible without any prior detector analysis and thereby we also avoid a time-consuming detector tomography.

d. Measured coincidences. In addition, an example of a measured coincidence statistics for outcomes (k_1, k_2) is shown in Fig. 5. There, we consider a state which is produced by the simplest conditioning to the 0th bin of the heralding TES (cf. Fig. 2). Based on this plot, let us briefly explain how these coincidences for (k_1, k_2) result in the statistics $c_{(N_0,\ldots,N_K)}$ for $(N_0, \ldots, N_K)$ and $K = 7$. The counts on the diagonal, $k_1 = k_2 = k$, of the plot yield $c_{(N_0,\ldots,N_K)}$ for $N_k = 2$ and $N_{k'} = 0$ for $k' \neq k$. For example, the highest counts are recorded for $(k_1, k_2) = (0, 0)$ in Fig. 5 which gives $c_{(2,0,\ldots,0)}$ when normalized to all counts. Off-diagonal combinations, $k_1 \neq k_2$, result in $c_{(N_0,\ldots,N_K)}$ for $N_{k_1} = N_{k_2} = 1$ and $N_k = 0$ otherwise. For example, the normalized sum of the counts for $(k_1, k_2) \in \{(0, 1), (1, 0)\}$ yields $c_{(1,1,0,\ldots,0)}$. As we have $N = 2$ TESs in our multiplexing scheme and $N_0 + \cdots + N_K = N$, these two cases already define the full distribution $c_{(N_0,\ldots,N_K)}$. The asymmetry in the counting statistics between the two detectors results in a small systematic error $\lesssim 1\%$; cf. also Appendix A. One should keep in mind that the counts are plotted in a logarithmic scale. For all other measurements of heralded multi-photon states, this error is in the same order.

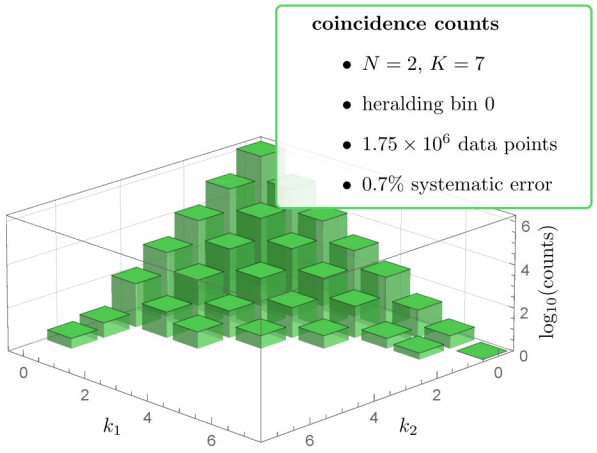

FIG. 5. (Color online) One example of measured coincidence counts is shown. k_n $(n = 1, 2)$ is the number of the bin for which the count was recorded. Some additional information on the statistics are given in the inset. The depicted state is produced by heralding on the 0th bin of the heralding TES in Fig. 2.

V. RESULTS OF THE DATA ANALYSIS

A. Heralded multi-photon states

Now, we perform an analysis on the first measured states to identify photon-number-based nonclassicality. Note that in Fig. 3 of Ref. [1], we analyzed the nonclassicality of this state in terms of condition (18). Here, let us focus on the idea to relating our measurement to the notion of sub-Poisson light, which has a convenient interpretation in terms of the photon-number statistics—as we will show. Moreover, in the next subsection, we will also compare the different criteria for sub-multinomial, -binomial, and -Poisson light.

We have already shown, in Sec. III (paragraph a.), the connection of the operator $:\mu:$ to the photon number statistics for the idealized scenario of photoelectric detection POVMs, $:\hat{\mu}: = :\hat{\Gamma}:/N = (\eta/N)\hat{n}$. Assuming this simple detector response, we can relate—in this ideal

case—the quantities

$$\langle{:}\hat{\mu}{:}\rangle = \frac{\eta}{N}\langle{:}\hat{n}{:}\rangle \text{ and } \langle{:}(\Delta\hat{\mu})^2{:}\rangle = \frac{\eta^2}{N^2}\langle{:}(\Delta\hat{n})^2{:}\rangle. \quad (29)$$

Recalling $:\hat{n}: = \hat{n}$, we see that $\langle:\hat{\mu}:\rangle$ is proportional to the mean photon-number in the approximation we apply here. Similarly, we can connect $\langle:(\Delta\hat{\mu})^2:\rangle$ to the normally-ordered photon-number fluctuations. They are non-negative for classical states and negative for sub-Poisson light. In Appendix B, we show for such idealized POVMs that we get for the heralding to the lth outcome from a two-mode squeezed-vacuum state,

$$|q\rangle = \sqrt{1-|q|^2}\sum_{n=0}^{\infty} q^n |n\rangle \otimes |n\rangle, \quad (30)$$

the following mean value and the variances:

$$\begin{aligned}\langle{:}\hat{\mu}{:}\rangle &= \frac{\eta}{N}\frac{\tilde{\lambda}+l}{1-\tilde{\lambda}},\\ \langle{:}(\Delta\hat{\mu})^2{:}\rangle &= \frac{\eta^2}{N^2}\frac{(\tilde{\lambda}+l)^2 - l(l+1)}{(1-\tilde{\lambda})^2},\end{aligned} \quad (31)$$

with a transformed squeezing parameter $\tilde{\lambda} = (1-\tilde{\eta})|q|^2$ and $\tilde{\eta}$ being the efficiency of the heralding TES. Note that for $\tilde{\lambda} \to 0$, we get the lth Fock state $|l\rangle$ (also given in Appendix B).

The results of our measurement are shown in the top panel of Fig. 6. We directly sampled the quantities in Eq. (16) from the measured statistics (see Appendix A for details on the error analysis), which yield the plotted quantities (see also paragraph around Eq. (20) and paragraph a. in Sec. III). The idealized theoretical modeling is additionally shown in the bottom part of Fig. 6. On the one hand, we do not observe nonclassicality when heralding to the 0th bin, which is expected as we condition on vacuum. On the other hand, we can observe nonclassicality for the conditioning to higher bins of the heralding TES. We have a linear relation between the normally ordered mean and variance of $:\hat{\mu}:$, which is consistent with the theoretical prediction of the idealized model; see Eq. (31). The higher the number of the heralding bin l, the larger the value of $\langle:\hat{\mu}:\rangle$ as the mean-photon number of Fock states increases with the number of photons, approximated by l and $\langle l|\hat{n}|l\rangle = l$. The normally-ordered variance of the photon-number for Fock states exhibits also a linear decrease to larger negativities with l (ideal case $\langle l|:(\Delta\hat{n}):|l\rangle\rangle = -l$). It is also obvious that the errors for the verification of nonclassicality with this particular test for sub-Poisson light, $\langle:(\Delta\mu)^2:\rangle < 0$, are quite large compared to Fig. 3 in Ref. [1]. We will discuss this discrepancy in more detail in the next subsection.

Here, let us already emphasize that the nonclassicality is verified with a single multiplexing step only. Moreover, we compared our data with a simple theoretical model and characterized the operation of the individual TESs in the previous section. We stress that our data processing neither needs nor uses any of this information. Our verification of nonclassicality is independent of the theoretical or reconstructed model of the TESs and the modeling of the PDC source.

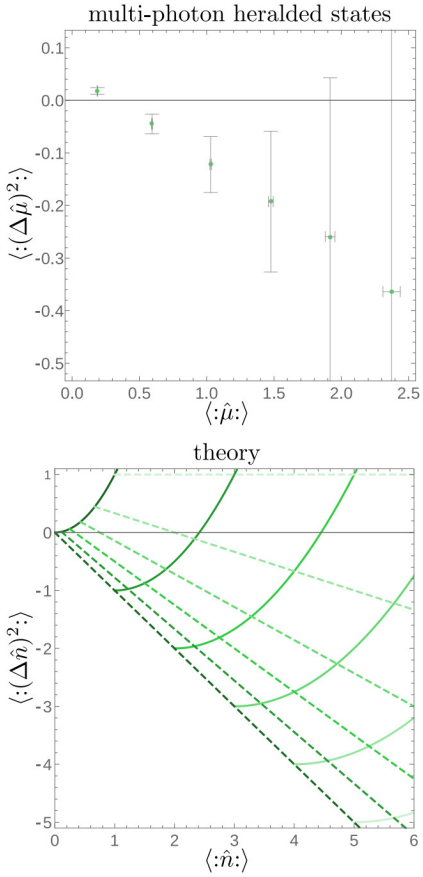

FIG. 6. (Color online) The top panel shows the experimental results of the analysis for the lth heralded state (increasing l from left to right and $l = 0, \ldots, 5$). The bottom plot shows the theoretical model for photon-number correlations [cf. Eq. (29)]. The solid quadratic curves show the dependence for varying $\tilde{\lambda}$ and fixed $0 \leq l \leq 5$ (lighter for increasing l). The dashed linear curves show the dependence for varying l and fixed $0 \leq \tilde{\lambda} \leq 0.5$ (lighter for increasing $\tilde{\lambda}$).

B. Varying pump power

So far, we have studied measurements for a fixed pump power of the PDC process. However, it is known that the quality of the heralded states depends on the squeezing parameter, which is a function of the pump power. For instance, in the limiting case of a vanishing squeezing, we have the optimal approximation of the heralded state to a Fock state. However, the rate of the probabilistic generation of that state converges to zero in the same

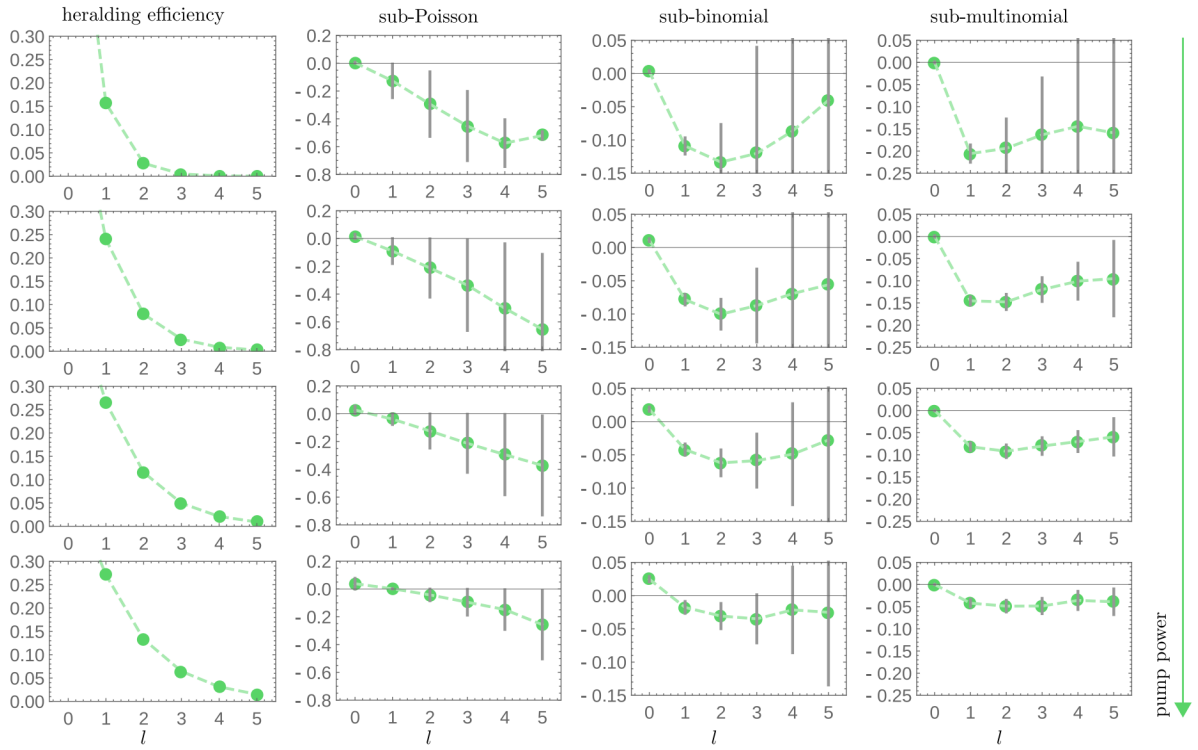

FIG. 7. (Color online) The results of our analysis are shown for different pump powers (increasing from top to bottom rows) as functions of the heralding bin l. The first column shows the success rate [Eq. (32)] for generating the lth multi-photon state. The second, third, and fourth columns depict the sub-Poisson, sub-binomial, and sub-multinomial nonclassicality criteria in Eqs. (34), (35), and (36), respectively. For a better overview, dashed lines connect the individual data points.

limit (Appendix B). Hence, we have additionally generated multi-photon states for different squeezing levels and analyzed their nonclassicality. The results are visualized in Fig. 7 and will be discussed in the following.

Suppose we measure the counts C_l for the lth bin of the heralding TES. The efficiency of generating this lth heralded state is simply given by

$$\eta_{\mathrm{gen}} = \frac{C_l}{\sum_l C_l}. \tag{32}$$

In our ideal model of a photon-number-resolving detector, we get from Appendix B that

$$\eta_{\mathrm{gen}} = \frac{1-|q|^2}{1-|q|^2(1-\tilde{\eta})}\left(\frac{\tilde{\eta}|q|^2}{1-|q|^2(1-\tilde{\eta})}\right)^l. \tag{33}$$

That is, the efficiency decays exponentially with l and the decay is stronger for smaller squeezing or pump power, also described by a decreasing $|q|^2$. In the left column of Fig. 7, we can observe this behavior. Note that the heralding to $l > 5$ is not studied as the number of such heralding events is too small for a proper statistical evaluation. It can be seen in all other parts of Fig. 7 that η_{gen} influences the significance of our results. That is, a smaller η_{gen} value naturally implies a larger error. This holds for increasing the heralding bin l as well as for decreasing the pump power.

In the second column in Fig. 7, labeled as "sub-Poisson", we study the nonclassicality in terms of the criterion

$$0 > N^2(N-1)\vec{f}^{\mathrm{T}} M^{(2)} \vec{f} \text{ for } \vec{f} = (0,1,\ldots,K)^{\mathrm{T}} \tag{34}$$

as well as $N = 2$ and $K = 7$. As we discussed in Sec. III, this relates to the notation of sub-Poisson light, including a correction term. Note that we use a different normalization for convenience; compare to Eq. (18). The third column in Fig. 7 shows the corresponding concept of "sub-binomial" light. This is verified through

$$0 > N^2(N-1)\vec{f}^{\mathrm{T}} M^{(2)} \vec{f} \text{ for } \vec{f} = (0,1,\ldots,1)^{\mathrm{T}}. \tag{35}$$

The last column is labeled as "sub-multinomial". It depicts the certified nonclassicality via the criterion

$$0 > N^2(N-1)\vec{f}_0^{\mathrm{T}} M^{(2)} \vec{f}_0, \tag{36}$$

where $\vec{f}_0$ is a normalized eigenvector to the minimal eigenvalue of $M^{(2)}$.

For all notations of nonclassicality under study, the heralding to the 0th bin is consistent with our expectation of a classical state, which also confirms that no fake-nonclassicality is detected. For instance, applying the Mandel parameter to the data of this 0th heralded stated without the corrections derived here [Eq. (26)], we would observe a negative value; see also a similar discussion in Refs. [9, 47]. The case of a Poisson or binomial statistics tend to be above zero, whereas the multinomial case is consistent with the value of zero. This expectation has been justified below Eq. (13).

A lot of information on the quantum-optical properties of the generated multi-photon ($l > 0$) light fields can be concluded from Fig. 7. Let us mention some of them by focusing on a comparison. We have the trend that the notion of sub-Poisson light has the least significant nonclassicality. This is due to the fact that the vector $\vec{f}$ in Eq. (34) assigns a higher contribution to the larger bin numbers. However, those contributions have lower count numbers, cf. Fig. 5, which consequently decreases the statistical significance. This effect is not present for sub-binomial light, which is described by a more or less balanced weighting of the different counts; see vector $\vec{f}$ in Eq. (35). However, this vector is still a fixed one. The optimal vector is naturally computed by the sub-multinomial criterion in Eq. (36). The quality of the verified nonclassicality is much better than for the other two scenarios of sub-Poisson and -binomial light in most of the cases. Let us mention that the normalized eigenvector to the minimal eigenvalue of the sampled matrix $M^{(2)}$ typically, but not necessarily yields the minimal propagated error. The comparative analysis of sub-Poisson, -binomial, and -multinomial light from a measurement with a single detection device would not be possible without the technique that has been elaborated in this work. As mentioned earlier, a lower pump power allows for the heralding of a state which is closer to an ideal Fock state, which results in higher mean negativities for decreasing pump powers. However, the heralding efficiency is reduced, which results in a larger error.

VI. SUMMARY

In summary, we constructed a detector-independent theory for a multiplexing scheme that employs arbitrary detectors for verifying nonclassicality of multi-photon states. We formulated the quantum-optical theory of such a detection layout. Further, we set up an experimental realization and applied our technique to the data.

In a first step, the theory was formulated. We proved that the measured click-counting statistics of such a scheme is always described by a quantum version of the multinomial statistics. Indeed, for classical light, we demonstrated that this probability distribution can be considered as a mixture of multinomial statistics. This bounds the minimal amount of fluctuations which can be observed for classical radiation fields. More precisely, the matrix of normally ordered moments, which can be directly sampled from data, is lower bounded by zero in such a scenario. As a particular example, the violation of this classical constraint was discussed for the second-order covariance matrix and it led to establishing the concept of sub-multinomial light. It was also determined that previous notions of nonclassicality, i.e, sub-Poisson and sub-binomial light, can be considered to be special cases of our general nonclassicality criteria.

In our second part, the experiment was analyzed. Our source produces correlated photon pairs by a parametric-down-conversion process. A heralding to the outcome of a detection of the idler photons with a transition-edge sensor produced multi-photon states in the signal beam. A single multiplexing step was implemented with a subsequent detection by two transition-edge sensors to probe the signal field. The complex function of these detectors was discussed by demonstrating their nonlinear response to the number of incident photons. Consequently, without worrying about this unfavorable feature, we applied our detector-independent nonclassicality criteria to our data. We verified the nonclassical character of the produced quantum light. The criterion of sub-multinomial light was shown to outperform its Poisson and binomial counterparts to the greatest possible extend.

In conclusion, we presented a supplementary study of our approach in Ref. [1] by performing an investigation of the considered detection schemes in the frame of quantized light fields. We generalized the method to include higher-order correlations which become more and more accessible with an increasing number of multiplexing steps. In addition, details of our data analysis and a simple theoretical model are presented in two appendices. We believe that our developed approach to verify quantum correlations with unspecified detectors without introducing fake-nonclassicality will pave the way towards the optical implementation of robust detection schemes for future quantum technologies.

ACKNOWLEDGMENTS

The project leading to this application has received funding from the European Union's Horizon 2020 research and innovation programme under grant agreement No 665148. A. E. is supported by EPSRC EP/K034480/1. J. J. R. is supported by the Netherlands Organization for Scientific Research (NWO). W. S. K is supported by EPSRC EP/M013243/1. S. W. N., A. L., and T. G are supported by the Quantum Information Science Initiative (QISI). I. A. W. acknowledges an ERC Advanced Grant (MOQUACINO). The authors thank Johan Fopma for technical support.

Note: This work includes contributions of the National Institute of Standards and Technology, which are not subject to U.S. copyright.

Appendix A: Data analysis and error propagation

For the application of our approach, we study in this appendix some data-analysis methods. Suppose we measure coincidence counts $C_{\vec{k}}$, with $\vec{k} = (k_1, \ldots, k_N) \in \{0, \ldots, K\}^N$ labeling the event that the nth detector yields the measurement outcome k_n. The total number of counts is given by $C = \sum_{\vec{k}} C_{\vec{k}} = \|C_{\vec{k}}\|$. Note that the data analysis is performed in terms of such arrays $C_{\vec{k}}$. Therefore, we use this multi-index notation to formulate this appendix to ensure reproducibility.

The numbers N_k—number of detectors that give the outcome k—can be also arranged in the $(K+1)$-dimensional multi-index $\vec{N} = (N_0, \ldots, N_K)$. The relation to $\vec{k}$ is given by the following function:

$$\vec{N} = \nu(\vec{k}) \stackrel{\text{def.}}{=} \sum_n \vec{e}_{k_n}, \tag{A1}$$

where $\vec{e}_k$ is the kth standard basis vector. Note that $\|\vec{N}\| = \sum_k N_k = N$. Then, the measured click-counting statistics (8) is formally written as

$$c_{(N_0,\ldots,N_K)} = c(\vec{N}) = \frac{1}{C} \sum_{\vec{k}:\nu(\vec{k})=\vec{N}} C_{\vec{k}}. \tag{A2}$$

A particular example was considered in Fig. 5 together with the discussion in paragraph d. of Sec. IV.

For a balanced splitting or multiplexing, all permutations $P_\sigma \vec{k}$ give the same count rates, $C_{P_\tau \vec{k}} = C_{\vec{k}}$, where P_τ is the operator which redistributes the components of $\vec{k}$ according to the permutation $\tau \in \mathcal{S}_N$. Hence, the deviation from this symmetry can be considered as a relative systematic error,

$$\varepsilon_{\text{sys}} = \sum_{\tau \in \mathcal{S}_N} \frac{\|C_{\vec{k}} - C_{P_\tau \vec{k}}\|}{C}. \tag{A3}$$

In combination with a relative statistical error $\varepsilon_{\text{stat}}$ for the estimate $\overline{f}$ of a quantity f, we have $f = \overline{f}(1 \pm [\varepsilon_{\text{stat}} + \varepsilon_{\text{sys}}]) = \overline{f} \pm \Delta f$.

In order the sample a quantity f, which is a function of the number of coincidences $\vec{N}$, we obtain

$$\overline{f} = \sum_{\vec{N}} f(\vec{N}) c(\vec{N}) = \frac{1}{C} \sum_{\vec{k}} f(\nu(\vec{k})) C_{\vec{k}}. \tag{A4}$$

The standard error of the mean is $\sigma(\overline{f}) = [(\overline{f^2} - \overline{f}^2)/(C-1)]^{1/2}$, which gives the relative statistical error $\varepsilon_{\text{stat}} = \sigma(\overline{f})/|\overline{f}|$. For example, we get for the moments $f(\vec{N}) = \vec{N}^{\vec{w}} = \prod_k N_k^{w_k}$:

$$f(\vec{N}) = \prod_k \left(\sum_n \delta_{k,k_n} \right)^{w_k} \tag{A5}$$

using $N_k = \vec{e}_k \cdot \nu(\vec{k})$ [cf. Eq. (A1)] and the Kronecker symbol δ.

Further note that a linear error propagation is favorable as the systematic error might exceed the statistical error. For instance, a matrix $M = \overline{M} \pm \Delta M$ and a given vector $\vec{f}$ yields via a linearly propagated error

$$\vec{f}^\dagger M \vec{f} = \vec{f}^\dagger \overline{M} \vec{f} \pm |\vec{f}|^\dagger \Delta M |\vec{f}|, \tag{A6}$$

where $|\cdot|$ acts component-wise on the vector $\vec{f}$. See also [47] for more details—especially for the case that $\vec{f}$ is an eigenvector of $\overline{M}$.

Appendix B: Theoretical Model

Let us analytically compute the quantities which are used as our simple theoretical model for the physical system under study. The PDC source produces a two-mode squeezed-vacuum state (30) ($|q|^2 < 1$), where the first mode is the signal and the second mode is the idler/herald. In our model, the heralding detector is supposed to be a photon-number-resolving detector with a quantum efficiency $\tilde{\eta}$. A multiplexing and a subsequent measurement with N photon-number-resolving detectors ($K = \infty$) are employed for the click counting. Each of the photon-number-resolving-detector's POVM elements is described by

$$:\hat{\pi}_k: = :\frac{(\eta\hat{n}/N)^k}{k!} e^{-\eta\hat{n}/N}:. \tag{B1}$$

In addition, we will make use of the relations $:e^{y\hat{n}}: = (1+y)^{\hat{n}}$ (cf., e.g., Ref. [81]) and

$$\begin{aligned} \partial_z^k :e^{[z-1]y\hat{n}}:|_{z=1} &=: (y\hat{n})^k :, \\ \frac{1}{k!}\partial_z^k :e^{[z-1]y\hat{n}}:|_{z=0} &=: \frac{(y\hat{n})^k}{k!} e^{-y\hat{n}}:. \end{aligned} \tag{B2}$$

For this model, we can conclude that the overall generating function for the two-mode squeezed-vacuum state reads

$$\begin{aligned} \Gamma(z, \vec{x}) &= \langle :e^{[z-1]\tilde{\eta}\hat{n}} \otimes e^{[\|\vec{x}\|-1]\eta\hat{n}/N}: \rangle \\ &= \frac{1-|q|^2}{1-|q|^2(1-\tilde{\eta}+\tilde{\eta}z)(1-\eta+\eta\|\vec{x}\|/N)}. \end{aligned} \tag{B3}$$

where $z \in [0,1]$ relates the heralding mode and the components of $\vec{x} \in [0,1]^N$ (recall: $\|\vec{x}\| = \sum_n x_n$) to the outcomes of the N detectors in the multiplexing scheme. From this generating function, we directly deduce the different properties that are used in this work for comparing the measurement with our model. The needed derivatives are

$$\begin{aligned} &\partial_{\vec{x}}^{\vec{k}} \partial_z^l \Gamma(z, \vec{x}) = \partial_{\|\vec{x}\|}^k \partial_z^l \Gamma(z, \vec{x}) \\ &= (1-|q|^2) l! k! \frac{\left[(\eta/N)|q|^2 z'\right]^k \left[\tilde{\eta}|q|^2 x'\right]^l}{\left[1-|q|^2 x' z'\right]^{k+l+1}} \\ &\quad \times \sum_{j=0}^{\min\{k,l\}} \frac{(k+l-j)!}{j!(k+j)!(l-j)!} \left[\frac{1-|q|^2 x' z'}{|q|^2 x' z'}\right]^j, \end{aligned} \tag{B4}$$

where $k=\|\vec{k}\|$, $x'=1-\eta+\eta\|\vec{x}\|/N$, and $z'=1-\tilde{\eta}+\tilde{\eta}z$. It is also worth mentioning that the case $N=1$ yields the result for photon-number-resolving detection without multiplexing.

The marginal statistics of the heralding detector reads

$$\begin{aligned}\tilde{p}_l =& \frac{1}{l!}\partial_z^l\Gamma(z,\vec{x})|_{z=0,x_1=\cdots=x_N=1}\\ =&\frac{1-|q|^2}{1-|q|^2(1-\tilde{\eta})}\left(\frac{\tilde{\eta}|q|^2}{1-|q|^2(1-\tilde{\eta})}\right)^l. \end{aligned}\tag{B5}$$

The marginal statistics of the nth detector is

$$\begin{aligned}&\frac{1}{k_n!}\partial_{x_n}^{k_n}\Gamma(1,\vec{x})|_{x_n=0,z=1=x_1=\cdots=x_{n-1}=x_{n+1}=\cdots=x_N}\\ =&\frac{1-|q|^2}{1-|q|^2(1-\eta/N)}\left(\frac{\eta|q|^2/N}{1-|q|^2(1-\eta/N)}\right)^{k_n}. \end{aligned}\tag{B6}$$

In addition, the case of no multiplexing ($N=1$ and $x\cong\vec{x}$) yields for the lth heralded state the following first and second normally ordered photon numbers:

$$\langle:(\eta\hat{n}):\rangle =\frac{1}{\tilde{p}_l l!}\partial_x\partial_z^l\Gamma(z,x)|_{z=0,x=1}=\eta\frac{l+\tilde{\lambda}}{1-\tilde{\lambda}},\tag{B7}$$

$$\begin{aligned}\langle:(\eta\hat{n})^2:\rangle =&\frac{1}{\tilde{p}_l l!}\partial_x^2\partial_z^l\Gamma(z,x)|_{z=0,x=1}\\ =&\eta^2\frac{(2(l+\tilde{\lambda})^2-l(l+1))}{(1-\tilde{\lambda})^2},\end{aligned}\tag{B8}$$

with $\tilde{\lambda}=(1-\tilde{\eta})|q|^2$. The corresponding photon distribution (i.e., for $\eta=1$) of the lth multi-photon state reads

$$\begin{aligned}\tilde{p}_{k|l} =&\frac{1}{\tilde{p}_l}\frac{1}{k!l!}\partial_x^k\partial_z^l\Gamma(z,x)|_{z=x=0}\\ =&\begin{cases}0 & \text{for}\quad k<l,\\ \binom{k}{l}(1-\tilde{\lambda})^{l+1}\tilde{\lambda}^{n-l} & \text{for}\quad k\geq l.\end{cases}\end{aligned}\tag{B9}$$

For $\tilde{\lambda}\to 0$, we have $\tilde{p}_{k|l}=\delta_{k,l}$ which is the photon statistics of the lth Fock state.

[1] J. Sperling, *et al.*, Detector-Independent Verification of Quantum Light (to be published).

[2] A. Einstein, Über einen die Erzeugung und Verwandlung des Lichtes betreffenden heuristischen Gesichtspunkt, Ann. Phys. (Leipzig) **17**, 132 (1905).

[3] G. S. Buller and R. J. Collins, Single-photon generation and detection, Meas. Sci. Technol. **21**, 012002 (2010).

[4] C. J. Chunnilall, I. P. Degiovanni, S. Kück, I. Müller, and A. G. Sinclair, Metrology of single-photon sources and detectors: A review, Opt. Eng. **53**, 081910 (2014).

[5] N. Gisin and R. Thew, Quantum communication, Nat. Photon. **1**, 165 (2007).

[6] J. H. Shapiro, The Quantum Theory of Optical Communications, IEEE J. Sel. Top. Quantum Electron. **15**, 1547 (2009).

[7] A. A. Semenov and W. Vogel, Fake violations of the quantum Bell-parameter bound, Phys. Rev. A **83**, 032119 (2011).

[8] I. Gerhardt, Q. Liu, A. Lamas-Linares, J. Skaar, V. Scarani, V. Makarov, and C. Kurtsiefer, Experimentally Faking the Violation of Bells Inequalities, Phys. Rev. Lett. **107**, 170404 (2011).

[9] J. Sperling, W. Vogel, and G. S. Agarwal, True photocounting statistics of multiple on-off detectors, Phys. Rev. A **85**, 023820 (2012).

[10] E. C. G. Sudarshan, Equivalence of Semiclassical and Quantum Mechanical Descriptions of Statistical Light Beams, Phys. Rev. Lett. **10**, 277 (1963).

[11] R. J. Glauber, Coherent and incoherent states of the radiation field, Phys. Rev. **131**, 2766 (1963).

[12] U. M. Titulaer and R. J. Glauber, Correlation functions for coherent fields, Phys. Rev. **140**, B676 (1965).

[13] L. Mandel, Non-classical states of the electromagnetic field, Phys. Scr. **T12**, 34 (1986).

[14] A. Miranowicz, M. Bartkowiak, X. Wang, Yu-xi Liu, and F. Nori, Testing nonclassicality in multimode fields: A unified derivation of classical inequalities, Phys. Rev. A **82**, 013824 (2010).

[15] E. Shchukin, Th. Richter, and W. Vogel, Nonclassicality criteria in terms of moments, Phys. Rev. A **71**, 011802(R) (2005).

[16] L. Mandel, Sub-Poissonian photon statistics in resonance fluorescence, Opt. Lett. **4**, 205 (1979).

[17] G. S. Agarwal and K. Tara, Nonclassical character of states exhibiting no squeezing or sub-Poissonian statistics, Phys. Rev. A **46**, 485 (1992).

[18] Th. Richter and W. Vogel, Nonclassicality of Quantum States: A Hierarchy of Observable Conditions, Phys. Rev. Lett. **89**, 283601 (2002).

[19] J. Sperling, W. Vogel, and G. S. Agarwal, Operational definition of quantum correlations of light, Phys. Rev. A **94**, 013833 (2016).

[20] C. Silberhorn, Detecting quantum light, Contemp. Phys. **48**, 143 (2007).

[21] R. H. Hadfield, Single-photon detectors for optical quantum information applications, Nat. Photon. **3**, 696 (2009).

[22] A. Luis and L. L. Sánchez-Soto, Complete Characterization of Arbitrary Quantum Measurement Processes, Phys. Rev. Lett. **83**, 3573 (1999).

[23] G. M. D'Ariano, L. Maccone, and P. Lo Presti, Quantum Calibration of Measurement Instrumentation, Phys. Rev. Lett. **93**, 250407 (2004).

[24] M. Lobino, D. Korystov, C. Kupchak, E. Figueroa, B. C. Sanders, and A. I. Lvovsky, Complete characterization of quantum-optical processes, Science **322**, 563 (2008).

[25] J. S. Lundeen, A. Feito, H. Coldenstrodt-Ronge, K. L. Pregnell, C. Silberhorn, T. C. Ralph, J. Eisert, M. B. Plenio, and I. A. Walmsley, Tomography of quantum detectors, Nat. Phys. **5**, 27 (2009).

[26] L. Zhang, A. Datta, H. B. Coldenstrodt-Ronge, X.-M. Jin, J. Eisert, M. B. Plenio, and I. A. Walmsley, Re-

cursive quantum detector tomography, New J. Phys. **14**, 115005 (2012).
[27] G. Brida, L. Ciavarella, I. P. Degiovanni, M. Genovese, A. Migdall, M. G. Mingolla, M. G. A. Paris, F. Piacentini, and S. V. Polyakov, Ancilla-Assisted Calibration of a Measuring Apparatus, Phys. Rev. Lett. **108**, 253601 (2012).
[28] J. Peřina, O. Haderka, V. Michálek, and M. Hamar, Absolute detector calibration using twin beams, Opt. Lett. **37**, 2475 (2012).
[29] M. Bohmann, R. Kruse, J. Sperling, C. Silberhorn, and W. Vogel, Direct calibration of click-counting detectors arXiv:1611.04779 [quant-ph].
[30] A. E. Lita, A. J. Miller, and S. W. Nam, Counting near-infrared single-photons with 95% efficiency, Opt. Express **16**, 3032 (2008).
[31] T. Gerrits, *et al.*, On-chip, photon-number-resolving, telecommunication-band detectors for scalable photonic information processing, Phys. Rev. A **84**, 060301(R) (2011).
[32] G. Brida, L. Ciavarella, I. P. Degiovanni, M. Genovese, L. Lolli, M. G. Mingolla, F. Piacentini, M. Rajteri, E. Taralli, and M. G. A. Paris, Quantum characterization of superconducting photon counters, New J. Phys. **14**, 085001 (2012).
[33] J. J. Renema, G. Frucci, Z. Zhou, F. Mattioli, A. Gaggero, R. Leoni, M. J. A. de Dood, A. Fiore, and M. P. van Exter, Modified detector tomography technique applied to a superconducting multiphoton nanodetector, Opt. Express **20**, 2806 (2012).
[34] L. Zhang, H. Coldenstrodt-Ronge, A. Datta, G. Puentes, J. S. Lundeen, X.-M. Jin, B. J. Smith, M. B. Plenio, and I. A. Walmsley, Mapping coherence in measurement via full quantum tomography of a hybrid optical detector, Nat. Photon. **6**, 364 (2012).
[35] K. Laiho, K. N. Cassemiro, D. Gross, and C. Silberhorn, Probing the Negative Wigner Function of a Pulsed Single Photon Point by Point, Phys. Rev. Lett. **105**, 253603 (2010).
[36] G. Brida, M. Genovese, M. Gramegna, A. Meda, F. Piacentini, P. Traina, E. Predazzi, S. Olivares, and M. G. A. Paris, Quantum state reconstruction using binary data from on/off photodetection, Adv. Sci. Lett. **4**, 1 (2011).
[37] E. Lantz, J.-L. Blanchet, L. Furfaro, and F. Devaux, Multi-imaging and Bayesian estimation for photon counting with EMCCDs, Mon. Not. R. Astron. Soc. **386**, 2262 (2008).
[38] R. Chrapkiewicz, W. Wasilewski, and K. Banaszek, High-fidelity spatially resolved multiphoton counting for quantum imaging applications, Opt. Lett. **39**, 5090 (2014).
[39] M. J. Applegate, O. Thomas, J. F. Dynes, Z. L. Yuan, D. A. Ritchie, and A. J. Shields, Efficient and robust quantum random number generation by photon number detection, Appl. Phys. Lett. **107**, 071106 (2015).
[40] E. Waks, E. Diamanti, B. C. Sanders, S. D. Bartlett, and Y. Yamamoto, Direct Observation of Nonclassical Photon Statistics in Parametric Down-Conversion, Phys. Rev. Lett. **92**, 113602 (2004).
[41] O. Haderka, J. Peřina, Jr., M. Hamar, and J. Peřina, Direct measurement and reconstruction of nonclassical features of twin beams generated in spontaneous parametric down-conversion, Phys. Rev. A **71**, 033815 (2005).
[42] R. Filip and L. Lachman, Hierarchy of feasible nonclassicality criteria for sources of photons, Phys. Rev. A **88**, 043827 (2013).
[43] I. I. Arkhipov, J. Peřina Jr., O. Haderka, A. Allevi, and M. Bondani, Entanglement and nonclassicality in four-mode Gaussian states generated via parametric down-conversion and frequency up-conversion, Sci. Rep. **6**, 33802 (2016).
[44] S.-H. Tan, L. A. Krivitsky, and B.-G. Englert, Measuring quantum correlations using lossy photon-number-resolving detectors with saturation, J. Mod. Opt. **63**, 276 (2015).
[45] M. Avenhaus, K. Laiho, M. V. Chekhova, and C. Silberhorn, Accessing Higher Order Correlations in Quantum Optical States by Time Multiplexing, Phys. Rev. Lett. **104**, 063602 (2010).
[46] A. Allevi, S. Olivares, and M. Bondani, Measuring high-order photon-number correlations in experiments with multimode pulsed quantum states, Phys. Rev. A **85**, 063835 (2012).
[47] J. Sperling, M. Bohmann, W. Vogel, G. Harder, B. Brecht, V. Ansari, and C. Silberhorn, Uncovering Quantum Correlations with Time-Multiplexed Click Detection, Phys. Rev. Lett. **115**, 023601 (2015).
[48] J.-L. Blanchet, F. Devaux, L. Furfaro, and E. Lantz, Measurement of Sub-Shot-Noise Correlations of Spatial Fluctuations in the Photon-Counting Regime, Phys. Rev. Lett. **101**, 233604 (2008).
[49] P.-A. Moreau, J. Mougin-Sisini, F. Devaux, and E. Lantz, Realization of the purely spatial Einstein-Podolsky-Rosen paradox in full-field images of spontaneous parametric down-conversion, Phys. Rev. A **86**, 010101(R) (2012).
[50] J. Sperling, T. J. Bartley, G. Donati, M. Barbieri, X.-M. Jin, A. Datta, W. Vogel, and I. A. Walmsley, Quantum Correlations from the Conditional Statistics of Incomplete Data, Phys. Rev. Lett. **117**, 083601 (2016).
[51] G. Zambra, A. Andreoni, M. Bondani, M. Gramegna, M. Genovese, G. Brida, A. Rossi, and M. G. A. Paris, Experimental Reconstruction of Photon Statistics without Photon Counting, Phys. Rev. Lett. **95**, 063602 (2005).
[52] W. N. Plick, P. M. Anisimov, J. P. Dowling, H. Lee, and G. S. Agarwal, Parity detection in quantum optical metrology without number-resolving detectors, New J. Phys. **12**, 113025 (2010).
[53] B. Kühn and W. Vogel, Unbalanced Homodyne Correlation Measurements, Phys. Rev. Lett. **116**, 163603 (2016).
[54] M. Cooper, M. Karpinski, and B. J. Smith, Quantum state estimation with unknown measurements, Nat. Commun. **5**, 4332 (2014).
[55] M. Altorio, M. G. Genoni, F. Somma, and M. Barbieri, Metrology with Unknown Detectors, Phys. Rev. Lett. **116**, 100802 (2016).
[56] H. Paul, P. Törmä, T. Kiss, and I. Jex, Photon Chopping: New Way to Measure the Quantum State of Light, Phys. Rev. Lett. **76**, 2464 (1996).
[57] P. Kok and S. L. Braunstein, Detection devices in entanglement-based optical state preparation, Phys. Rev. A **63**, 033812 (2001).
[58] D. Achilles, C. Silberhorn, C. Śliwa, K. Banaszek, and I. A. Walmsley, Fiber-assisted detection with photon number resolution, Opt. Lett. **28**, 2387 (2003).
[59] M. J. Fitch, B. C. Jacobs, T. B. Pittman, and J. D. Franson, Photon-number resolution using time-multiplexed single-photon detectors, Phys. Rev. A **68**, 043814 (2003).

[60] J. Řeháek, Z. Hradil, O. Haderka, J. Peřina, Jr., and M. Hamar, Multiple-photon resolving fiber-loop detector, Phys. Rev. A **67**, 061801(R) (2003).

[61] P. L. Kelley and W. H. Kleiner, Theory of Electromagnetic Field Measurement and Photoelectron Counting, Phys. Rev. **136**, A316 (1964).

[62] A. Ilyin, Generalized binomial distribution in photon statistics, Open Phys. **13**, 41 (2014).

[63] M. Pleinert, J. von Zanthier, and G. S. Agarwal, Quantum signatures of collective behavior of a coherently driven two atom system coupled to a single-mode of the electromagnetic field, arXiv:1608.00137 [quant-ph].

[64] F. M. Miatto, A. Safari, and R. W. Boyd, Theory of multiplexed photon number discrimination, arXiv:1601.05831 [quant-ph].

[65] G. Harder, T. J. Bartley, A. E. Lita, S. W. Nam, T. Gerrits, and C. Silberhorn, Single-Mode Parametric-Down-Conversion States with 50 Photons as a Source for Mesoscopic Quantum Optics, Phys. Rev. Lett. **116**, 143601 (2016).

[66] J. Sperling, W. Vogel, and G. S. Agarwal, Sub-Binomial Light, Phys. Rev. Lett. **109**, 093601 (2012).

[67] T. J. Bartley, G. Donati, X.-M. Jin, A. Datta, M. Barbieri, and I. A. Walmsley, Direct Observation of Sub-Binomial Light, Phys. Rev. Lett. **110**, 173602 (2013).

[68] C. Lee, S. Ferrari, W. H. P. Pernice, and C. Rockstuhl, Sub-Poisson-Binomial Light, Phys. Rev. A **94**, 053844 (2016).

[69] T. Meany, M. Gräfe, R. Heilmann, A. Perez-Leija, S. Gross, M. J. Steel, M. J. Withford, and A. Szameit, Laser written circuits for quantum photonics, Laser Photon. Rev. **9**, 1863 (2015).

[70] R. Heilmann, J. Sperling, A. Perez-Leija, M. Gräfe, M. Heinrich, S. Nolte, W. Vogel, and A. Szameit, Harnessing click detectors for the genuine characterization of light states, Sci. Rep. **6**, 19489 (2016).

[71] G. S. Agarwal and E. Wolf, Calculus for Functions of Noncommuting Operators and General Phase-Space Methods in Quantum Mechanics. I. Mapping Theorems and Ordering of Functions of Noncommuting Operators, Phys. Rev. D **2**, 2161 (1970); *ibid.*, II. Quantum Mechanics in Phase Space, Phys. Rev. D **2**, 2187 (1970); *ibid.*, III. A Generalized Wick Theorem and Multitime Mapping, Phys. Rev. D **2**, 2206 (1970).

[72] J. Sperling, W. Vogel, and G. S. Agarwal, Correlation measurements with on-off detectors, Phys. Rev. A **88**, 043821 (2013).

[73] See Ch. 8 in W. Vogel and D.-G. Welsch, *Quantum Optics* (Wiley-VCH, Weinheim, 2006).

[74] T. Lipfert, J. Sperling, and W. Vogel, Homodyne detection with on-off detector systems, Phys. Rev. A **92**, 053835 (2015).

[75] A. Eckstein, A. Christ, P. J. Mosley, and C. Silberhorn, Highly Efficient Single-Pass Source of Pulsed Single-Mode Twin Beams of Light, Phys. Rev. Lett. **106**, 013603 (2011).

[76] K. Laiho, K. N. Cassemiro, and Ch. Silberhorn, Producing high fidelity single photons with optimal brightness via waveguided parametric down-conversion, Opt. Express **17**, 22823 (2009).

[77] S. Krapick, H. Herrmann, V. Quiring, B. Brecht, H. Suche and Ch. Silberhorn, An efficient integrated two-color source for heralded single photons, New J. Phys. **15**, 033010 (2013).

[78] A. J. Miller, A. E. Lita, B. Calkins, I. Vayshenker, S. M. Gruber, and S. W. Nam, Compact cryogenic self-aligning fiber-to-detector coupling with losses below one percent, Opt. Express **19**, 9102 (2011).

[79] K. D. Irwin, An application of electrothermal feedback for high resolution cryogenic particle detection, Appl. Phys. Lett. **66**, 1998 (1995).

[80] P. C. Humphreys, B. J. Metcalf, T. Gerrits, T. Hiemstra, A. E. Lita, J. Nunn, S. W. Nam, A. Datta, W. S. Kolthammer, and I. A. Walmsley, Tomography of photon-number resolving continuous-output detectors, New J. Phys. **17**, 103044 (2015).

[81] J. Sperling, W. Vogel, and G. S. Agarwal, Quantum state engineering by click counting, Phys. Rev. A **89**, 043829 (2014).